Journal of The Korean Astronomical Society
46: 243 ∼ 251, 2013 December

http://dx.doi.org/10.5303/JKAS.2013.46.6.243
ISSN:1225-4614
http://jkas.kas.org

INTRINSIC BRIGHTNESS TEMPERATURE OF COMPACT RADIO SOURCES AT 86GHZ

Sang-Sung Lee
Korea Astronomy and Space Science Institute, 776 Daedukdae-ro, Yusong, Daejon 305-348, Korea
E-mail : sslee@kasi.re.kr
(Received September 13, 2013; Revised October 29, 2013; Accepted November 4, 2013)

ABSTRACT

We present results on the intrinsic brightness temperature of a sample of compact radio sources observed at 86 GHz using the Global Millimeter VLBI Array. We use the observed brightness temperatures at 86 GHz and the observed superluminal motions at 15 GHz for the sample in order to constrain the characteristic intrinsic brightness temperature of the sample. With a statistical method for studying the intrinsic brightness temperatures of innermost jet cores of compact radio sources, assuming that all sources have the same intrinsic brightness temperature and the viewing angles of their jets are around the critical value for the maximal apparent speed, we find that sources in the sample have a characteristic intrinsic brightness temperature, $T_0 = 4.8^{+2.6}_{-1.5} \times 10^9$ K, which is lower than the equipartition temperature for the condition that the particle energy equals to the magnetic field energy. Our results suggest that the VLBI cores seen at 86 GHz may be representing a jet region where the magnetic field energy dominates the total energy in the jet.

Key words : Galaxies: nuclei — quasars: relativistic jets — radio: galaxies

1. INTRODUCTION

Compact radio sources are generally defined as radio sources whose flux density at an intermediate radio frequency, e.g., ∼ 1 GHz, is dominated by the emission of a single bright region within ∼ 1 kpc in size (Blandford & Königl 1979). Compact radio sources usually have flat radio spectra and exhibit pronounced radio variability. Moreover, due to the lager ratio of optical to radio flux of the compact radio sources than of steep-spectrum sources, these objects have been easily identified.

Radio emission from parsec-scale jets in compact radio sources consists of optically thin synchrotron emission, and characterized by their spectral and polarization properties and significant inverse-Compton emission (see Marscher 1990; Hughes & Miller 1991). The flat spectrum of the radio emission is generally interpreted as due to superposition of incoherent synchrotron radiation from a non-thermal distribution of relativistic electrons located in several distinct components (Kellermann & Pauliny-Toth 1969; Marscher 1995). These components form the innermost compact structure, the compact jet base at sub-parsec scales, and the bright emission regions at parsec scales of the jet. The physical processes of the formation of inner jets that connect the nucleus to the observed radio jet, their acceleration to relativistic speeds, and strong collimation to large scales (pc to kpc) have been extensively investigated but remain poorly understood (e.g., Marscher 2006; Lobanov & Zensus 2006; Lobanov 2007).

Readhead (1994) suggested that parsec-scale jets are in an equipartition condition that the energy density in relativistic particles is equal to that in magnetic fields (Burbidge & Burbidge 1957). He found that the radio sources may radiate at an equipartition brightness temperature around 5×10^{10} K in most circumstances. Recent studies have shown that extended radio lobes are indeed at equipartition (Croston et al. 2005), and the relativistic jets are at equipartition in their median-low state (Homan et al. 2006). However when the relativistic jets are in their maximum state, the brightness temperatures are a factor of 4 larger, implying the energy in their radiating particle is $\geq 10^5$ times larger than the energy in magnetic fields, based on the relation of the energy and brightness temperature as proposed in Readhead (1994): $\eta = u_p/u_B = (T_{\rm eq}/T_{\rm b})^{-17/2}$, where u_p,u_B are the energy densities of the radiating particles and the magnetic field, respectively, $T_{\rm eq} \simeq 5 \times 10^{10}$ K is the equipartition brightness temperature, and $T_{\rm b}$ is the observed brightness temperature. It is very difficult to measure intrinsic properties of extragalactic compact radio sources because the jets of compact radio sources are highly relativistic and therefore Doppler boosted (Blandford & Königl 1979; Lind & Blandford 1985). The physical aspects of the jet can be parameterized by the Lorentz factor $\gamma_{\rm j}$, the intrinsic brightness temperature T_0, and the angle to the line of sight $\theta_{\rm j}$. From these intrinsic physical properties, one can calculate the Doppler factor δ, the apparent jet speed $\beta_{\rm app}$, and the observed brightness

temperature $T_{\rm b}$:

$$\delta = \frac{1}{\gamma_{\rm j}(1-\beta{\rm cos}\theta_{\rm j})}, \quad (1)$$

$$\beta_{\rm app} = \frac{\beta{\rm sin}\theta_{\rm j}}{1-\beta{\rm cos}\theta_{\rm j}}, \quad (2)$$

$$T_{\rm b} = T_0\delta, \quad (3)$$

where $\beta = (1-{\gamma_{\rm j}}^{-2})^{1/2}$ is the speed of jet in the rest frame of the source (units of c).

Observed brightness temperatures ($T_{\rm b}$) of compact radio jets can be used to study the intrinsic physical properties of the relativistic jets. One application is to test accelerating and decelerating jet models (Marscher 1995) by investigating the change in the observed brightness temperatures measured at various radio frequencies (e.g., 2 – 86 GHz). Under equipartition conditions between jet particle and magnetic field energy densities, the position shift of the brightest jet components of VLBI images (VLBI cores) between two frequencies can be predicted (Lobanov 1998). The brightness temperatures in the rest frame of the sources and the predicted core shift should be able to test the inner jet models.

Another application is to obtain the intrinsic brightness temperatures of VLBI cores by using the observed brightness temperature $T_{\rm b}$ and the maximum apparent jet speed $\beta_{\rm app}$. A method developed by Homan et al. (2006) was applied to the 2 cm survey data (Kellermann et al. 2004) in order to determine the intrinsic physical properties of prominent AGN (Cohen et al. 2007). They found that VLBI cores observed at 15 GHz are near equipartition in their median–low state, resulting in intrinsic brightness temperatures of $T_0 = 3\times10^{10}$ K.

The method can be applied to VLBI survey data at different frequencies, with the maximum apparent jet speeds taken from Kellermann et al. (2004), in order to constrain the intrinsic brightness temperature at these frequencies. In this paper, we combine the observed brightness temperature data from a global 86 GHz VLBI imaging survey (Lee et al. 2008) and proper-motion data from the 2 cm VLBA survey. In Section 2, the theory and its application to the 2 cm VLBA survey are reviewed. In Section 3, we present our results using the 86 GHz VLBI survey. In Section 4, we discuss the interpretation of the intrinsic brightness temperatures at various frequencies.

2. INTRINSIC BRIGHTNESS TEMPERATURE AT 15 GHz

2.1 Methodology

Following Homan et al. (2006), we assume that a compact radio source contains an ideal relativistic jet, which is narrow and straight with no bends between the VLBI core and the jet components. Of course, some jets are not straight and $\theta_{\rm j}$ is not the same in the core and in the moving jet components. The celebrated example and evidence of the jet bending are found in 3C 279 (Homan et al. 2003; Abdo et al. 2010). However, as long as superluminal motion is observed, the motion must be close to the line of sight, and angular changes of the motion could be highly magnified due to projection effect. A jet with an intrinsic bend of only a few degrees could be observed as a right-anlge bending jet (Cohen et al. 2007).

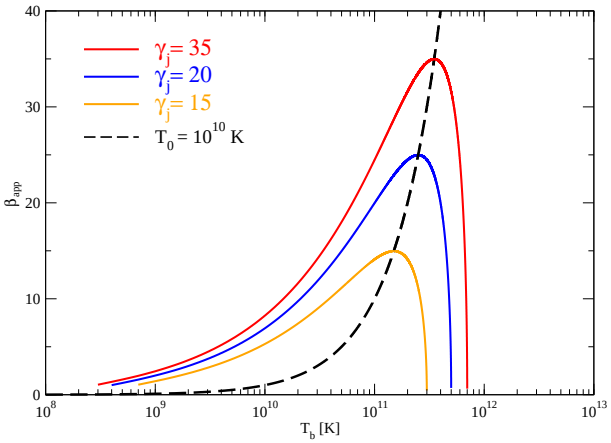

Fig. 1.— Plot of the apparent jet speed $\beta_{\rm app}$ with the observed brightness temperature $T_{\rm b}$ for a single intrinsic brightness temperature of $T_0 = 1\times10^{10}$ K and several values of Lorentz factors $\gamma_{\rm j} = 15, 20, 35$. The dashed line represents where sources observed at the critical angle would lie on this plot. The solid line represents the possible apparent speeds of a $\gamma_{\rm j}$ source with intrinsic brightness temperature given by T_0.

In this case, we can also assume that the maximum speed of the jet component is the same as the speed of the jet flow through the jet core. The flow speed of the jet is usually different from the pattern speed of the jet in some low-luminosity sources. However, in those sources which are bright and straight, the pattern speeds are the same as the flow speeds. For simplicity, we make two further assumptions:

1. The intrinsic brightness temperature T_0 of all jets are the same, and
2. The viewing angels of their jets are around the critical value $\theta_{\rm c} = \arccos\beta$ for the maximal apparent speed at a given β.

Under the assumptions above, one can relate the observed brightness temperature to the maximum jet speed:

$$\delta \simeq \beta_{\rm app} \quad (4)$$

and

$$T_{\rm b} \simeq \beta_{\rm app} T_0. \quad (5)$$

This resultant simple relation between the observed brightness temperature and the apparent maximum jet speed is illustrated in Fig. 1. From Eqs. 1 and 2,

one can also relate the apparent jet speed $\beta_{\rm app}$ to the Doppler factor δ and the Lorentz factor $\gamma_{\rm j}$:

$$\beta_{\rm app} = \sqrt{(\delta\gamma_{\rm j}\beta)^2 - (\delta\gamma_{\rm j} - 1)^2}. \quad (6)$$

This relation is illustrated as three solid lines in Figure 1, for the maximum and minimum possible Doppler factors $\delta_{\rm max} = 1/\gamma_{\rm j}$ and $\delta_{\rm min} = 1/(\gamma_{\rm j} - \sqrt{\gamma_{\rm j}{}^2 - 1})$. The lines show actually the apparent speeds as functions of $T_{\rm b}$ for jets with Lorentz factors of $\gamma_{\rm j}$ =15, 20, and 25. Homan et al. (2006) found that from the simulation of a relativistically beamed population of 1000 fictional compact radio sources with given T_0 and $\gamma_{\rm j}$, the dashed line divided the 1000 compact radio sources into two groups: one group of about 750 sources in the right and below, and another group of about 250 sources in the left and above. The viewing angles of 750 sources in the right and below are smaller than the critical angle, and their Doppler factors are large. Their proper motions are small due to their viewing angle.

2.2 Application to 15 GHz Data

By combining the 2 cm VLBA survey data and the proper motion data of AGN jets, Homan et al. (2006) found an intrinsic brightness temperature of $T_0 \simeq 3\times10^{10}$ K of the sources in their sample when the sources are in their median-low (25%-median) brightness temperature state, that is for median brightness temperatures of a lower half sample of observed brightness temperaturs obtained from multi-epoch observations of individual AGN. This value for T_0 is close to the equipartition temperature under the condition that the particle energy equals to the magnetic field energy. However, for maximum observed brightness temperatures, they also found a characteristic intrinsic brightness temperature of 2×10^{11} K of their sample, which is brighter than the equipartition temperature by a factor of 4. This implies that, in the maximum brightness state, the energy in radiating particles exceeds the energy in the magnetic field by a factor of $\sim 10^5$. They suggest that at the innermost regions of the jet, injection or acceleration of particles should maintain the energy in the radiating particles dominant over the energy in the magnetic field.

3. INTRINSIC BRIGHTNESS TEMPERATURE AT 86 GHz

3.1 A Global 86 GHz VLBI Survey Data

In an attempt to investigate intrinsic brightness temperature for sources observed at 86 GHz, we used the observed brightness temperatures of VLBI cores at 86 GHz from a large global 86 GHz VLBI survey of compact radio sources (Lee et al. 2008). The survey data consist of total intensity images with a typical image FWHM restoring beam of approximately 40 μas. This corresponds to a scale of < 0.1 parsecs at typical redshifts z≅1 for our sample AGNs. We used Gaussian fit to the VLBI core component of each jet to determine a rest-frame core brightness temperature $T_{\rm b}$ for each jet according to

$$T_{\rm b} = 1.22\times10^{12}\frac{S_{\rm tot}}{d^2\nu^2}(1+z)\ {\rm K}, \quad (7)$$

where $S_{\rm tot}$ is the fitted core flux density in Janskys at ν=86 GHz, d is the FWHM dimensions of the fitted circular core components in milliarcseconds. In determining the FWHM d of a core component, the resolution limit of the determination was taken into account. So, the minimum resolvable size of a component in an image is given by

$$d_{\rm min} = \frac{2^{1+\beta/2}}{\pi}\left[\pi ab\ln 2\ln\frac{SNR}{SNR-1}\right]^{1/2}, \quad (8)$$

where a and b are the axes of the restoring beam, SNR is the signal-to-noise ratio, and β is a weighting function, which is 0 for natural weighting or 2 for uniform weighting. When $d < d_{\rm min}$, the uncertainties should be estimated with $d = d_{\rm min}$. If $d < d_{\rm min}$, then the lower limit of $T_{\rm b}$ is obtained with $d = d_{\rm min}$.

3.2 VLBA Data

Since there are no reliable measurements of the apparent jet speeds at 86 GHz, we used the apparent jet speeds from the 2cm survey and the MOJAVE survey (Kellermann et al. 2004; Lister et al. 2009, 2013), thereby assuming that the apparent jet speeds at 15 and 86 GHz are similar each other. We selected the fastest proper motions for each source from the MOJAVE survey (Lister et al. 2009, 2013), assuming that the speeds are maximum values of individual sources. For some sources whose proper motions are not available in the MOJAVE survey, we used the apparent speeds from the 2cm survey (Kellermann et al. 2004), and we only considered those speeds that are ranked as "excellent" (E) or "good" (G) by their criteria. We found that apparent jet speeds at 15 GHz are available for 98 of the sources in the 86 GHz survey,

In order to constrain the characteristic intrinsic brightness temperature at 15 GHz for our sample, we obtained the maximum observed brightness temperatures ($T_{\rm b}^{\rm 15GHz,max}$) and the 25%-median brightness temperatures ($T_{\rm b}^{\rm 15GHz,25\%med}$) from Kovalev et al. (2005). Table 1 lists the observed brightness temperatures at 15 and 86 GHz for the selected target sources, with the optical class and redshift obtained from Véron-Cetty & Véron (2006). The final sample contains 98 sources, consisting of 7 galaxies, 20 BL Lac objects, 70 quasars, and one unidentified source according to the optical class.

Table 1.
Observed brightness temperatures

Name	Type	z	$\beta_{\rm app}$ [c]	$T_{\rm b}^{\rm 15GHz,max}$ [K]	$T_{\rm b}^{\rm 15GHz,25\%med}$ [K]	$T_{\rm b}^{\rm 86GHz}$ [K]
0003−066	B	0.347	8.39 ± 0.39	>4.60e+11	8.07e+10	>2.60e+10
0007+106	G	0.089	1.20 ± 0.07	9.05e+11	1.82e+11	>1.20e+10
0016+731	Q	1.781	8.23 ± 0.34	>7.24e+12	1.14e+11	>1.80e+11
0048−097	B	...	0.00 ± 0.00	>7.31e+12	>2.44e+11	2.50e+10
0106+013	Q	2.107	24.40 ± 3.90	>3.87e+12	8.83e+11	1.70e+11
0119+041	Q	0.637	0.50 ± 1.60	>1.86e+11	1.04e+11	>1.40e+10
0119+115	Q	0.570	18.58 ± 0.82	3.37e+11	1.50e+11	>5.90e+10
0133+476	Q	0.859	15.40 ± 1.20	>1.91e+13	7.14e+11	2.40e+11
0149+218	Q	1.32	18.40 ± 1.90	>1.40e+12	5.80e+11	5.10e+10
0202+149	Q	0.405	15.88 ± 0.75	>1.53e+12	1.82e+11	>4.80e+10
0202+319	Q	1.466	10.10 ± 1.00	>2.67e+12	1.10e+12	7.90e+10
0212+735	Q	2.367	6.58 ± 0.18	1.08e+12	2.00e+11	>2.70e+09
0224+671	Q	0.523	13.69 ± 0.56	>3.94e+11	>3.94e+11	>6.60e+10
0234+285	Q	1.207	22.00 ± 1.10	>3.83e+12	>4.51e+11	2.40e+11
0238−084	G	0.005	0.39 ± 0.02	>3.83e+12	>4.51e+11	>2.20e+10
0300+470	B	...	0.00 ± 0.00	>8.46e+11	>8.46e+11	2.90e+10
0316+413	G	0.017	0.29 ± 0.02	1.45e+11	1.45e+11	4.70e+10
0333+321	Q	1.263	13.05 ± 0.16	>5.11e+12	2.64e+11	1.40e+11
0336−019	Q	0.852	24.40 ± 1.60	>3.24e+12	4.51e+11	5.60e+10
0355+508	Q	1.52	1.90 ± 1.60	>9.77e+11	>6.59e+11	1.20e+11
0415+379	G	0.049	8.14 ± 0.31	>7.63e+11	1.56e+11	4.10e+10
0420+022	Q	2.277	8.51 ± 0.98	5.62e+11	3.02e+11	6.70e+10
0420−014	Q	0.915	5.76 ± 0.59	>5.18e+13	>2.12e+12	1.90e+11
0422+004	B	0.310	0.39 ± 0.19	>1.38e+12	>1.36e+12	>5.60e+10
0430+052	G	0.033	6.43 ± 0.24	>9.19e+11	>1.04e+11	9.80e+10
0440−003	Q	0.844	0.59 ± 0.15	2.31e+11	6.87e+10	>5.20e+10
0458−020	Q	2.291	13.56 ± 0.82	1.82e+12	8.17e+11	1.20e+11
0528+134	Q	2.07	17.33 ± 0.55	>2.06e+13	1.11e+12	>2.50e+11
0529+075	Q	1.254	18.00 ± 1.10	>1.91e+10	>1.48e+10	>1.30e+11
0552+398	Q	2.363	1.63 ± 0.10	1.16e+12	6.01e+11	2.20e+11
0607−157	Q	0.324	1.20 ± 0.83	>1.08e+13	1.49e+12	2.90e+10
0642+449	Q	3.408	8.52 ± 0.41	>2.84e+13	4.32e+12	1.60e+11
0707+476	Q	1.292	-2.80 ± 1.70	5.33e+11	2.67e+11	7.10e+10
0716+714	B	...	0.00 ± 0.00	>1.85e+13	>3.60e+11	3.60e+11
0727−115	Q	1.591	31.20 ± 0.60	>9.93e+12	>9.61e+11	1.40e+10
0735+178	B	0.424	5.05 ± 0.61	>6.99e+11	>1.34e+11	2.40e+10
0736+017	Q	0.191	13.79 ± 0.20	>2.51e+12	5.09e+11	1.00e+11
0738+313	Q	0.630	10.70 ± 1.20	>6.54e+11	>7.37e+10	3.60e+10
0748+126	Q	0.889	14.57 ± 0.56	>2.66e+12	9.06e+11	1.60e+11
0804+499	Q	1.432	1.17 ± 0.23	>2.94e+12	1.04e+12	6.20e+10
0814+425	B	0.530	0.00 ± 0.00	>1.40e+12	>1.09e+11	2.30e+10
0823+033	B	0.506	12.88 ± 0.49	>3.01e+12	>5.29e+11	5.00e+10
0827+243	Q	0.941	19.80 ± 1.30	1.93e+12	6.23e+11	>2.10e+11
0836+710	Q	2.218	21.10 ± 0.77	6.18e+12	2.97e+11	>1.70e+11
0850+581	Q	1.322	12.70 ± 4.10	>1.09e+11	>5.30e+10	3.20e+10
0851+202	B	0.306	15.13 ± 0.43	>4.80e+12	5.08e+11	2.00e+11
0906+015	Q	1.018	22.08 ± 0.47	6.20e+12	6.43e+11	>1.40e+11
0917+624	Q	1.446	12.10 ± 1.20	2.74e+11	9.44e+10	4.00e+10
0945+408	Q	1.252	20.21 ± 0.95	>3.07e+12	1.67e+11	5.00e+10
0954+658	B	0.367	12.74 ± 0.83	>9.06e+11	>9.06e+11	>9.50e+10

Table 1.
(Continued)

Name	Type	z	$\beta_{\rm app}$ [c]	$T_{\rm b}^{15\ {\rm GHz,max}}$ [K]	$T_{\rm b}^{15\ {\rm GHz,25\%med}}$ [K]	$T_{\rm b}^{86\ {\rm GHz}}$ [K]
1012+232	Q	0.565	9.00 ± 0.60	>2.48e+12	4.13e+11	3.90e+10
1101+384	B	0.031	0.28 ± 0.05	2.19e+11	6.14e+10	2.10e+10
1128+385	Q	1.733	1.10 ± 0.50	>4.94e+12	5.30e+11	8.10e+10
1150+497	Q	0.334	17.50 ± 2.00	>4.94e+12	5.30e+11	1.40e+11
1156+295	Q	0.729	24.60 ± 1.90	4.95e+12	2.60e+11	2.60e+11
1219+285	B	0.102	9.12 ± 0.79	>1.43e+11	>7.39e+10	1.60e+10
1226+023	Q	0.158	14.86 ± 0.17	>5.60e+12	>4.73e+11	8.50e+10
1228+126	G	0.004	0.03 ± 0.00	>4.52e+11	7.68e+10	1.80e+10
1253−055	Q	0.538	20.57 ± 0.79	>2.42e+13	5.53e+12	>8.90e+11
1308+326	Q	0.997	27.50 ± 1.20	>2.93e+12	2.26e+11	1.80e+11
1502+106	Q	1.833	17.55 ± 0.90	>3.22e+12	>1.32e+12	>2.70e+11
1508−055	Q	1.191	6.20 ± 1.20	>7.84e+11	3.76e+11	4.60e+10
1510−089	Q	0.360	28.00 ± 0.60	>5.60e+12	3.20e+11	>7.00e+10
1546+027	Q	0.412	12.10 ± 1.20	>2.76e+12	2.83e+11	>2.10e+10
1548+056	Q	1.422	11.60 ± 1.70	>1.03e+12	3.13e+11	>1.00e+11
1606+106	Q	1.226	19.08 ± 0.86	>2.65e+12	2.26e+11	>1.50e+11
1637+574	Q	0.751	13.61 ± 0.89	>1.33e+12	8.54e+11	3.20e+11
1642+690	Q	0.751	14.53 ± 0.26	>3.19e+12	>3.18e+11	1.60e+11
1652+398	B	0.033	0.87 ± 0.21	6.81e+10	5.22e+10	1.40e+09
1655+077	Q	0.621	14.80 ± 1.10	>7.37e+11	1.42e+11	1.00e+11
1739+522	Q	1.379	9.08 ± 4.64	3.77e+12	1.61e+11	3.90e+11
1741−038	Q	1.057	6.64 ± 1.74	>2.03e+13	1.35e+12	1.90e+11
1749+096	B	0.320	7.90 ± 0.75	>1.85e+13	>1.74e+12	6.10e+11
1800+440	Q	0.663	15.49 ± 0.32	>9.35e+12	7.02e+11	1.70e+11
1803+784	B	0.680	10.80 ± 1.20	2.71e+12	6.00e+11	8.00e+10
1807+698	B	0.050	0.09 ± 0.01	>3.92e+11	1.18e+11	>1.00e+11
1823+568	B	0.663	26.20 ± 2.60	>5.34e+12	>7.04e+11	1.40e+11
1828+487	Q	0.692	13.06 ± 0.14	>2.78e+12	2.55e+11	2.60e+10
1901+319	Q	0.635	0.90 ± 0.70	7.34e+11	>3.21e+11	3.20e+10
1921−293	Q	0.352	4.20 ± 1.30	2.75e+12	4.49e+11	3.90e+10
1923+210	U	...	0.00 ± 0.00	2.75e+12	4.49e+11	5.60e+10
1928+738	Q	0.303	8.16 ± 0.21	2.37e+12	3.19e+11	4.70e+10
1957+405	G	0.056	0.27 ± 0.04	2.37e+12	3.19e+11	2.80e+10
2007+777	B	0.342	0.30 ± 0.10	>1.06e+12	>1.81e+11	>3.70e+11
2013+370	B	...	12.53 ± 0.34	>1.06e+12	>1.81e+11	1.80e+11
2037+511	Q	1.687	3.78 ± 0.53	8.33e+11	6.07e+11	4.20e+11
2121+053	Q	1.941	11.64 ± 0.74	>1.24e+13	2.63e+12	8.70e+10
2128−123	Q	0.501	6.00 ± 0.62	>3.37e+11	>1.29e+11	2.30e+09
2134+004	Q	1.932	5.07 ± 0.32	>1.31e+12	1.97e+11	>4.60e+10
2155−152	Q	0.672	18.10 ± 1.80	>8.77e+11	>6.53e+11	2.00e+10
2200+420	B	0.069	9.95 ± 0.72	2.26e+12	>5.81e+11	>5.50e+12
2201+315	Q	0.298	8.28 ± 0.10	>2.77e+12	>1.06e+11	5.00e+10
2216−038	Q	0.901	6.75 ± 0.70	7.04e+11	>1.05e+11	5.80e+09
2223−052	Q	1.404	20.33 ± 0.65	>6.53e+12	>1.42e+12	7.30e+10
2234+282	Q	0.795	5.10 ± 2.20	>5.13e+11	4.20e+10	4.40e+10
2251+158	Q	0.859	13.79 ± 0.49	>3.37e+12	4.20e+11	>1.30e+11
2255−282	Q	0.927	6.00 ± 0.95	>2.24e+13	4.93e+12	2.00e+10
2345−167	Q	0.576	11.46 ± 0.76	>1.39e+12	2.80e+11	1.10e+09

3.3 Constraining Intrinsic Brightness Temperature

Fig. 2 shows plots of the apparent speed $\beta_{\rm app}$ versus the observed brightness temperature $T_{\rm b}$ for our sample. The top panel is a plot of $\beta_{\rm app}$ versus the maximum observed brightness temperatures at 15 GHz for each source in our sample. The dashed line indicates sources at the critical angle which have $T_0 = 1.2 \times 10^{11}$ K, and the solid grey line was calculated using the same value for T_0. The value of T_0 was chosen to have about 75% of the sources in the right of and below the dashed line, which is the same criterion for choosing the value of T_0 as in Homan et al. (2006). The middle panel is for sources in their median-low (25% median) state. This is the median of the lowest half of the brightness temperature observations for a given source as defined in Homan et al. (2006). The 25% median determined in this critera represents a typical low brightness state for each source at 15 GHz. We found a characteristic intrinsic brightness temperature of $T_0 = 2.0 \times 10^{10}$ K for the 25% median state. The intrinsic temperatures chosen at 15 GHz for our sample (98 sources) are very close to those for the sample (106 sources) of Homan et al. (2006). This implies that two samples are statistically similar and hence suitable for applying this method.

The bottom panel of Fig. 2 is a similar plot for the observed brightness temperatures at 86 GHz for each source in our sample. The value of $T_0 = 4.8 \times 10^9$ K was chosen to have about 75% of the sources in the right of and below the dashed line. Since other choices for the simulation parameters described in Homan et al. (2006) give a very similar distribution of $\beta_{\rm app}$ vs $T_{\rm b}$ and have fractions between 60% and 80% of sources with their viewing angles smaller than the critical angle, we take the corresponding values of $T_0 = 3.3 \times 10^9$ K for a 80% fraction and $T_0 = 7.4 \times 10^9$ K for a 60% fraction as the range of uncertainty for T_0.

Fig. 3 shows plots similar to Fig. 2 with sources divided into three groups: quasars, BL Lac objects, and galaxies. Galaxies have lower apparent jet speeds, whereas quasars and BL Lac objects are widely spread in speed.

3.4 Doppler Factor

The narrow range of intrinsic brightness temperatures determined at 15 GHz (median-low state) and 86 GHz enables us to derive Doppler factors for the sources in our sample according to Eq. 3. Figs. 4a and 4b show the distributions of estimated Doppler factors for the 15 GHz (25% median) data and the 86 GHz data. The distributions have the mean values of 31.2 and 24.1 (excluding one value exceeding 1000) with the medians of 16.1 and 14.6 for each data, respectively. This implies that Doppler factors derived with the data at 15 GHz and 86 GHz for our sample of sources are slightly different from each other. The Doppler factors of the VLBI core at 86 GHz are lower than those

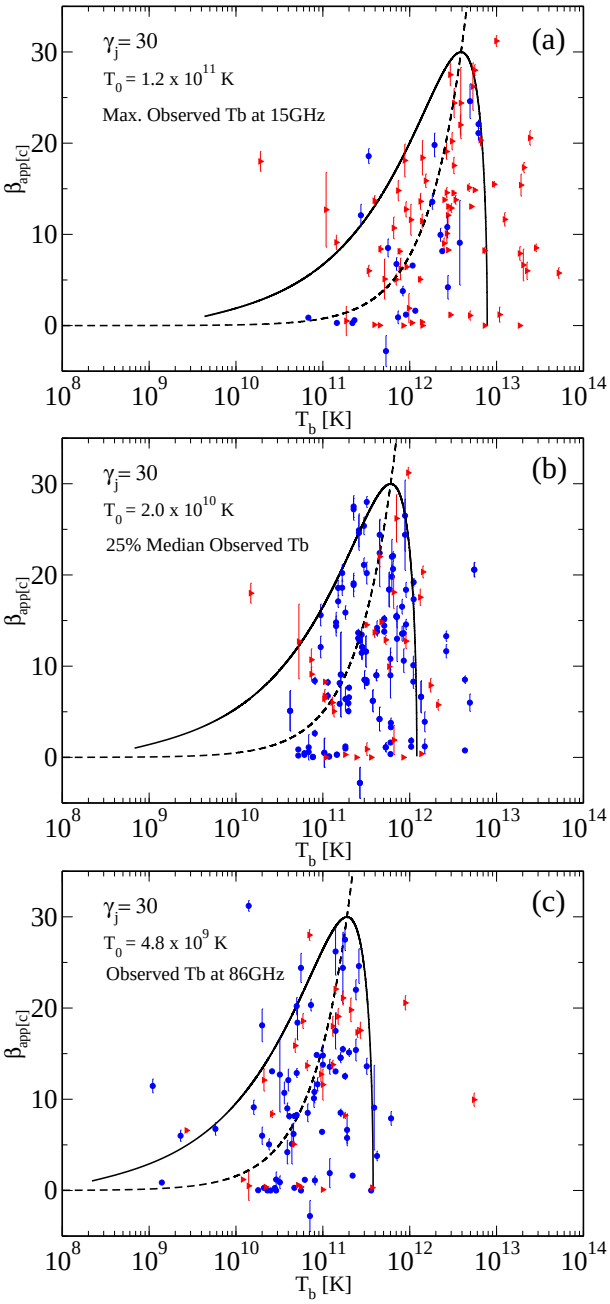

Fig. 2.— Plots of apparent jet speed versus observed brightness temperature for the sources in our sample. (a) and (b) plots are for the 15 GHz data. (c) plot is for the 86 GHz data. Lower limits of brightness temperatures are indicated by right triangle, and solid circles represent measurements. The dashed line represents sources observed at the critical angle that have the intrinsic brightness temperature of $T_0 = 1.2 \times 10^{11}$ K (a), $T_0 = 2.0 \times 10^{10}$ K (b), and $T_0 = 4.8 \times 10^9$ K (c). The solid grey line represents the possible apparent speeds of a $\gamma_{\rm j} = 30$ source with the corresponding intrinsic brightness temperatures.

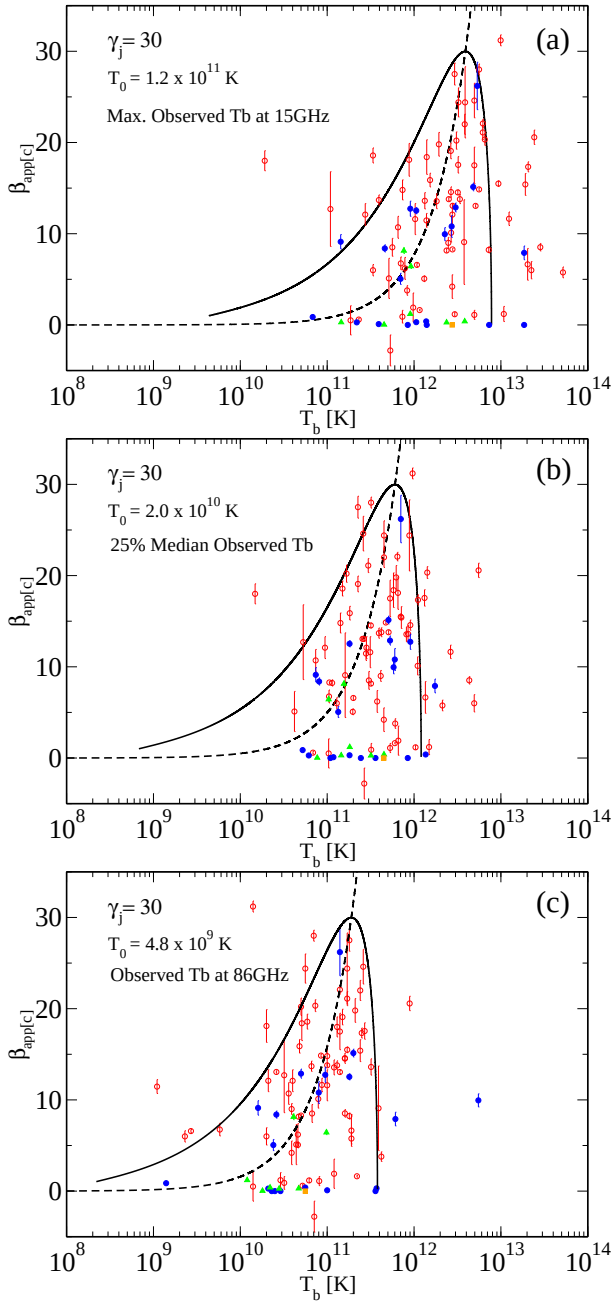

Fig. 3.— Similar plots as Fig. 2 except for the symbols: red open circles represent quasars; blue solid circles represent BL Lac objects; green triangles represent galaxies; one orange square represents unidentified source.

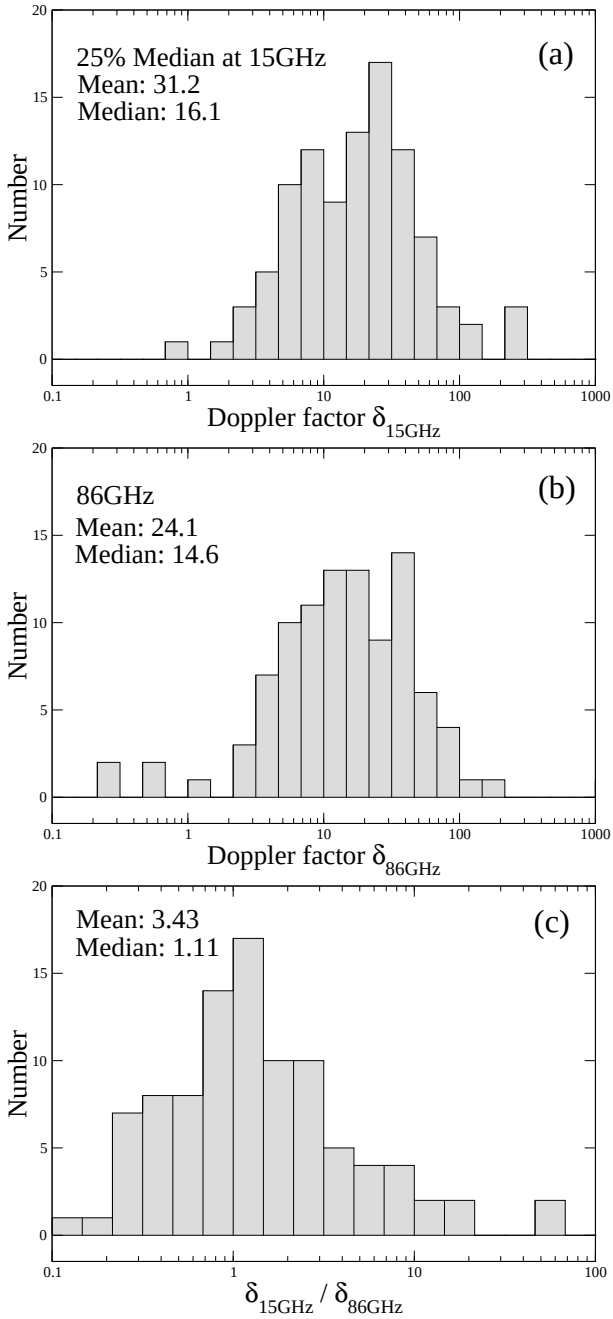

Fig. 4.— Distributions of Doppler factors at (a) 15 GHz and (b) 86 GHz, and of (c) their ratio. Mean and median values of each distribution are shown in each plot.

at 15 GHz. Fig. 4c shows the distribution of the ratio of Doppler factors at 15 GHz and 86 GHz for all sources in our sample. The distribution peaks at a value higher than unity, and has mean and median values of 3.43 and 1.11, implying that for many sources the estimated Doppler factors are higher for the 15 GHz jets than for the 86 GHz VLBI cores. Taking into account Eq. 4, higher Doppler factors indicate faster apparent jet speeds for sources whose viewing angles are close to the critical value θ_c for maximal apparent jet speed.

4. DISCUSSION

It is interesting that the plots β_{app} versus T_b in Figs. 2b and 2c show similar trends although few

sources are far beyond the solid curve in Fig. 2c. There are few sources having low brightness and fast apparent speeds. As discussed in Cohen et al. (2007), this implies that for the fastest jet components in many sources, the pattern speeds are closely related with the flow speeds. If the pattern and flow speeds were independent, then it is difficult to imagine such a trend in $\beta_{\rm app}$ versus $T_{\rm b}$. If some sources have fast pattern speeds with slow flow speeds, then they may be placed to the left of the solid line. This may be the case for the few sources located in the area of Fig. 2c.

As discussed in Homan et al. (2006), the chosen value of T_0 should be considered as a lower bound on the characteristic value. This is because there are more lower limits of observed brightness temperatures than measurements in Fig. 2a. For our sample $T_0 > 1.2 \times 10^{11}$ K when sources have their maximum brightness temperature. Therefore sources should be well away from equipartition. However, for the median-low state in Fig. 2b, there are fewer limits of the observed temperatures than measurements. We may consider the chosen value of T_0 the characteristic median-low intrinsic brightness temperature. For our sample $T_0 = 2.0 \times 10^{10}$ K. This value of T_0 is similar to the brightness temperature under an equipartition condition.

For the 86 GHz data, there are similar number of lower limits as the median-low plot, so it seems reasonable to take the characteristic intrinsic brightness temperature to be $T_0 = 4.8 \times 10^9$ K. This value is lower by a factor of $\sim$4 than the median-low intrinsic brightness temperature at 15 GHz. We note that the apparent decrease in brightness temperature between the 15 GHz and 86 GHz cases cannot be attributed to scatter in the plots, since the real ranges of the intrinsic brightness temperate in both cases are 1.6×10^{10} K $< T_0 < 3.1 \times 10^{10}$ K and 3.3×10^9 K $< T_0 < 7.4 \times 10^9$ K for the 15 GHz and 86 GHz cases, respectively, using the 60%- and 80%-fraction criteria.

This is lower-than-equipartition temperature implying that the VLBI cores seen at 86 GHz may be representing a jet region where the magnetic field energy dominates the total energy in the jet. Using Eq. 5 of Readhead (1994), we estimate that the 86 GHz VLBI core regions have 4.5×10^8 times more energy in magnetic fields as in radiating particles. In these circumstances we may expect conversion of magnetic field energy into the kinetic energy of particles in the jet. Since the 86 GHz VLBI cores should be located the inner regions of the jet in contrast to the 15 GHz cores and jets, taking into account the opacity effect of a relativistic jet (Lobanov 2007; Lobanov & Zensus 2006), we may also expect that the intrinsic brightness temperature will increase as we go down-stream of the jet. Applying similar estimates to the 15 GHz data, we found $1/\eta \simeq 2.4 \times 10^3$, implying the ratio between the energy in the magnetic fields and in their radiating particles may change by an order of 5 as the relativistic jet moves from the 86 GHz VLBI core regions to the 15 GHz jet regions.

The increase of the intrinsic brightness temperature may result in the increase of apparent jet speeds from the jet core of radio galaxies and BL Lac objects as reported by Lister et al. (2013). Fig. 13 of Lister et al. (2013) may imply that the apparent jet speeds at 15 GHz (in the outer region of the jet) are faster than those at 86 GHz (in the inner region), which is consistent with our results of Doppler factor in Section 3.4. Although positive correlation of speed with core distance needs to be confirmed based on a complete AGN sample, we may expect that the relativistic jets of AGNs may accelerate on moving away from the central engine with corresponding increase in the intrinsic brightness temperature. This also agrees with the results of Doppler factors. Some observational tests for the jet acceleration model will be discussed in a separate paper.

The difference in the intrinsic temperatures T_0 deduced at 15 GHz and 86 GHz may imply that only a small number of sources will be suitable for VLBI at higher frequencies (e.g., ≥ 300 GHz).

5. CONCLUSIONS

- The 86 GHz global VLBI survey has yielded the observed brightness temperatures for 98 sources with available apparent jet speeds and observed brightness temperatures at 15 GHz from the 2 cm VLBA survey and MOJAVE program. On applying the T_0-constraining method, we find that the intrinsic brightness temperature is $T_0 = 4.8^{+2.6}_{-1.5} \times 10^9$ K for the VLBI cores seen at 86 GHz.
- The Doppler factors estimated with the constrained intrinsic brightness temperatures tend to be higher for the jets seen at 15 GHz than for the VLBI cores seen at 86 GHz. It is likely that Doppler factor increases down-stream of a relativistic jet.
- The VLBI cores at 86 GHz in our sample may be such that the magnetic field energy in the jet converts into the kinetic energy of particles. Moving outwards, down stream of the jet, the intrinsic brightness temperature will increase.

ACKNOWLEDGMENTS

I would like to thank the anonymous referee for important comments and suggestions which have enormously improved the manuscript. The VLBA is an instrument of the National Radio Astronomy Observatory, which is a facility of the National Science Foundation operated under cooperative agreement by Associated Universities, Inc.. This work was supported by Global Research Collaboration and Networking program of Korea Research Council of Fundamental Science & Technology (KRCF).

REFERENCES

Abdo, A. A., Ackermann, M., Ajello, M., Axelsson, M., Baldini, L., Ballet, J., Barbiellini, G., Bastieri, D., Baughman, B. M., Bechtol, K., et al. 2010, A Change in the Optical Polarization Associated with a γ-Ray Flare in the Blazar 3C279, Nature, 463, 919

Blandford, R. D., & Königl, A. 1979, Relativistic Jets as Compact Radio Sources, ApJ, 232, 34

Burbidge, G. R., & Burbidge, E. M. 1957, The Sources of Radio Emission in NGC 5128 and NGC 1316, ApJ, 125, 1

Cohen, M. H., Lister, M. L., Homan, D. C., Kadler, M., Kellermann, K. I., Kovalev, Y. Y., & Vermeulen, R. C. 2007, Relativistic Beaming and the Intrinsic Properties of Extragalactic Radio Jets, ApJ, 658, 232

Croston, J. H., Hardcastle, M. J., Harris, D. E., Belsole, E., Birkinshaw, M., & Worrall, D. M. 2005, An X-Ray Study of Magnetic Field Strengths and Particle Content in the Lobes of FR II Radio Sources, ApJ, 626, 733

Homan, D. C., Lister, M. L., Kellermann, K. I., Cohen, M. H., Ros, E., Zensus, J. A., Kadler, M., & Vermeulen, R. C. 2003, Jet Collimation in Action: Realignment on Kiloparsec Scales in 3C 279, ApJ, 589, L9

Homan, D. C., Kovalev, Y. Y., Lister, M. L., Ros, E., Kellermann, K. I., Cohen, M. H., Vermeulen, R. C., Zensus, J. A., & Kadler, M. 2006, Intrinsic Brightness Temperatures of AGN Jets, ApJ, 642, L115

Hughes, P. A., & Miller, L. 1991, Introduction: Synchrotron and Inverse-Compton Radiation, Beams and Jets in Astrophysics, 1

Kellermann, K. I., & Pauliny-Toth, I. I. K. 1985, The Spectra of Opaque Radio Sources, ApJ, 295, 358

Kellermann, K. I., Lister, M. L., Homan, D. C., Vermeulen, R. C., Cohen, M. H., Ros, E., Kadler, M., Zensus, J. A., & Kovalev, Y. Y. 2004, Sub-Milliarcsecond Imaging of Quasars and Active Galactic Nuclei. III. Kinematics of Parsec-Scale Radio Jets, ApJ, 609, 539

Kovalev, Y. Y., Kellermann, K. I., Lister, M. L., Homan, D. C., Vermeulen, R. C., Cohen, M. H., Ros, E., Kadler, M., Lobanov, A. P., Zensus, J. A., Kardashev, N. S., Gurvits, L. I., Aller, M. F., & Aller, H. D. 2005, Sub-Milliarcsecond Imaging of Quasars and Active Galactic Nuclei. IV. Fine-Scale Structure, AJ, 130, 2473

Lee, S.-S., Lobanov, A. P., Krichbaum, T. P., Witzel, A., Zensus, J. A., Bremer, M., Greve, A., & Grewing, M. 2008, A Global 86 GHz VLBI Survey of Compact Radio Sources, AJ, 136, 159

Lind, K. R., & Blandford, R. D. 1985, Semidynamical Models of Radio Jets - Relativistic Beaming and Source Counts, ApJ, 295, 358

Lister, M. L., Cohen, M. H., Homan, D. C., Kadler, M., Kellermann, K. I., Kovalev, Y. Y., Ros, E., Savolainen, T., & Zensus, J. A. 2009, MOJAVE: Monitoring of Jets in Active Galactic Nuclei with VLBA Experiments. VI. Kinematics Analysis of a Complete Sample of Blazar Jets, AJ, 138, 1874

Lister, M. L., Aller, M. F., Aller, H. D., Homan, D. C., Kellermann, K. I., Kovalev, Y. Y., Pushkarev, A. B., Richards, J. L., Ros, E., & Savolainen, T. 2013, MOJAVE. X. Parsec-Scale Jet Orientation Variations and Superluminal Motion in AGN, AJ, in press (arXiv:1308.2713)

Lobanov, A. P. 1998, Ultracompact Jets in Active Galactic Nuclei, A&A, 330, 79

Lobanov, A. P., & Zensus, J. A. 2006, Extragalactic Relativistic Jets and Nuclear Regions in Galaxies, astro-ph/0606189

Lobanov, A. P. 2007, Compact Jets as Probes for Sub-Parsec Scale Regions in AGN, Ap&SS, 311, 263

Marscher, A. P. 1990, Interpretation of Compact Jet Observations, *Parsec-scale radio jets*, ed. Zensus & Peason (Cambridge: Cambridge University Press), 236

Marscher, A. P. 1995, Probes of the Inner Jets of Blazars, Proceedings of the National Academy of Science, 92, 11439

Marscher, A. P. 2006, Relativistic Jets in Active Galactic Nuclei, AIP Conf. Proc. 856: Relativistic Jets: The Common Physics of AGN, Microquasars, and Gamma-Ray Bursts, 1

Véron-Cetty, M.-P., & Véron, P. 2006, A Catalogue of Quasars and Active Nuclei: 12th Edition, A&A, 455, 773

Readhead, A. C. S. 1994, Equipartition Brightness Temperature and the Inverse Compton Catastrophe, ApJ, 426, 51